BJES Basrah Journal for Engineering Sciences

Basrah Journal for Engineering Sciences, Vol. 24, No. 2, (2024), 50-61

Original Article

Journal homepage: www.bjes.edu.iq
ISSN (Online): 23118385, ISSN (Print): 18146120

Vibration Signal Analysis Under Varying Machine Speed Using Spectral Correlation

Mohanad M. Matrood [1, *], Jaafar K. Alsalaet [2]

[1,2] *Department of Mechanical Engineering, College of Engineering, University of Basrah, Basrah, Iraq*
E-mail addresses: mohanadmajeed92@gmail.com , Jaafar.ali@uobasrah.edu.iq
Received: 18 June 2024; Accepted: 7 August 2024; Published: 17 August 2024

Abstract

Monitoring the health of rotating machinery is essential to ensure system safety, achieve cost savings, and enhance overall reliability. The requirement for a reliable and clear method of identifying defects has prompted the development of several monitoring techniques. They utilize vibration, measurement of the motor's current signature, and acoustic emission data in the process of condition monitoring. The MFS (machinery fault simulator) equipment was used to determine bearing faults using vibration signal analysis. MFS conducts simulations and investigations of many bearing issues, including those occurring in the inner race, outer race, and balls. An accelerometer (type B & K 4366) was connected to a data acquisition device (IDAC-6C) to record vibration signals under different operating conditions. Furthermore, a tachometer equipped with an LCD display is employed to measure the rotational speed. Four types of defects in ball bearing (Koyo 1205C3 type) were studied, the slot in outer race with size 0.196 mm, the slot in inner race with size 0.191 mm, in ball with size 0.196 mm in additional to compound defect. In this paper, spectral correlation technique was employed to detect defects in ball bearings running at varying speed, along with spectral coherence and the corresponding Enhanced Envelope Spectrum (EES) in frequency-order domain and order-order domain. The results show that the adopted methods, that are used to analyze the real vibration signals for diagnosis the defected ball bearings, are suitable, accurate and less processing time for varying speed. The processing time of the FastACP method used to analyze the signals in order-order domain is less than that of the adopted method in the frequency-order domain for any defect type. Overall, using the FastACP method in the order-order domain significantly reduced processing time by approximately 27% compared to the adopted method in the frequency-order domain under varying speed conditions.

Keywords: Vibration signal analysis, Bearing fault detection, Cyclo-non-stationary signals, Spectral correlation.

https://doi.org/10.33971/bjes.24.2.7

1. Introduction

The vibration signal is used for achieving the monitoring and identifying fault using the conventional signal processing approaches [1]. In healthy monitoring conditions, the measured signal is usually considered as stationary signal for the sequent analysis. Because of the noise and load fluctuation in defective state, non-stationary signal may be created in utmost actual conditions [2-5]. The cyclo-stationary method is an efficient tool for analyzing the non-stationery signal and it is applied to extract characteristic of signal, monitor state, and identify defect [6, 7]. Also, the signal of defected machine has non-stationary property, which delivers a possible improvement for cyclo-stationary method [8, 9]. Through the cyclo-stationary (CS) analysis, the important unseen characteristic info can be shown, and the various information represents the variable defect situations.

Usually, the signal has periodic or multi-periodic statistical characteristics are denoted as “cyclo-stationary (CS)” or “periodic stationary". The rotary machine, that runs with rotational motion, will create periodic-signal at standard operational conditions and it begins to vibrate, when the faults or defects occur in rotary machine. The vibration signal generated in this case is denoted as a “modulation signal”. Its second-order statistics (mostly cyclic autocorrelation function, spectral-correlation-function, and spectral-coherency-function) introduce the periodicity therefore it is observed as a cyclo-stationary signal [10]. Several papers dealt with using cyclo-stationary signal processes to diagnosis the vibration signals of intact and defected rotating machines [11-23]. For example, some researches dealt with the defect in gears such as [11, 15, 17 and 19]. On other side, the papers [12, 13, 14 and 20] considered faults in bearing. The cyclo-stationarity signal processes were analyzed and discussed in papers [16, 18, 21-23].

Gardner et al. [24] introduced a brief literature survey dealing with cyclo-stationarity and discussed them from different fields. They used “spectral correlation approach” for analyzing cyclo-non-stationary vibration signals of rotating machines when the rotation speed is variable, also in [23, 25-28].

On the other side, signals that exhibit a concealed periodicity associated with the angle of a shaft can be characterized as exhibiting cyclo-stationary in the temporal domain when subjected to constant speed operating conditions. Nevertheless, when subjected to different speed circumstances, the impulses associated with the rotating speed of the shaft exhibit a lack of cyclo-stationary over time, and the carriers associated with time no longer exhibit cyclo-stationary in terms of angle. Therefore, these entities are characterized as nonstationary. The aforementioned characteristic is recognized as the definitive representation of the signal emitted by rolling element bearings when subjected

to different operational circumstances. Despite the absence of time or angle-cyclo-stationary in the signals, there is still an underlying periodicity present in the signal.

The cyclo-non- stationary signals are analyzed by using the Frequency-Order SC (FOSC) method. To analyze cyclo-non-stationary signals, the Frequency-Order spectral-correlation (FOSC) method to shift the signal in the angle-domain. Otherwise, the signal can be resampled entirely in the angle domain to produce Order-Order spectral-correlation (OOSC) [23, 28]. Li et al. [29] used sparse code shrinkage algorithm to de-noise the measured signal to get enhanced results. Zhang et al. [30] controlled the involvement of each spectral frequency line for emphasizing the defect signature. Also, Smith et al. [31] developed a band selection tool to capture cyclo-stationarity established on the strength of target cyclic frequency components in the spectrum of the log envelope.

The spectral-correlation denotes the power distribution of the signal relating to the spectral frequency and cyclic frequency, while spectral-coherence is the weighted version of spectral-coherence and tends to magnify weak cyclo-stationary signals and both are used to analyze cyclo-stationary signals. These methods are able to reveal hidden periodicities that are masked by stronger signals and random noise and they can be displayed in the bi-variable map such as frequency-frequency, order-frequency, or order-order domains. The Enhanced Envelope Spectrum (EES) can be obtained by integrating the bi-variable over the spectral frequency.

One reason for the restriction of cyclic spectral analysis is the high computation costs involved in the analysis of cyclo-stationary signals. Generally, the spectral correlation may be costly to calculate in certain instances such that it becomes impractical to apply for quick troubleshooting and daily analysis. Several studies have been prepared to minimize computation costs. Roberts et al. [32] suggested the FFT Accumulation Method (FAM) and the Strip-Spectral-Correlation Algorithm (SSCA) but the estimation error of this method is very high because of degradation of the statistical performance of the estimator [32]. The Strip-Spectral-Correlation Algorithm offers some computational saving over the FFT Accumulation Method at the expense of a degraded signal-to-noise ratio of the output [32, 33]; and it needs huge memory, therefore it is used for to analyze small-sized signals only.

Antoni et al. [34] estimated the spectral correlation using new suggested algorithm named the Fast-Spectral-Correlation (FSC) algorithm. Their new algorithm based on analyzing the Short Time Fourier Transform (STFT) lines around a certain spectral frequency to extract the Spectral-Correlation. Since they introduced this method, the Fast-Spectral-Correlation (FSC) has become a standard method for spectral correlation estimation in vibration field.

On other side, Borghesani and Antoni [35] suggested new faster method to reduce the computation cost but the method requires double the memory. The disadvantages of their new method are numerical instability, the inconsistent results depending on the cyclic frequency range.

The Averaged Cyclic Periodogram method is one of the most important methods to compute spectral-correlation and it bases on the weighted overlapped segment averaging, which is applied in spectrum averaging [32, 37]. Despite ACP calculations can be accelerated by using power-of-two processing window length to calculate the Short Time Fourier Transform (STFT), the method computation cost is still very high due to the calculations of shifted STFTs for the whole range of cyclic frequency [32, 36]. In this work, the Fast Averaged Cyclic Periodogram method, that proposed by Alsalaet [36], is used to analyze the measured vibration signal of defected ball bearing. Experimentally, four types of defects in ball bearings are employed in this work (Outer Race Slot, Inner Race Slot, Ball Slot and Combined Defects).

2. Theoretical background

2.1. Vibration signal under constant speed

Emerging defects in rolling bearings are generally resulting from a local material loss such as pitting, spalling, corrosion, rubbing, contamination in contact surfaces inner race, outer race, balls. If a rolling body touches the defect, impulse with short duration will generate and this impulse signal leads to excite several resonances of the bearing structural [36]. Duo to repeat of these impulses during bearing operation, a sequence of impulse responses, whose temporal spacing effects by the defect kind and bearing dimensions, will be generated. Also, this impulse responses series is probably amplitude modulated because of the transitory of the defect through the load zone. Normally, defects in outer race generate a uniform amplitude modulation for fixed outer race and existence of a radial load, while defects in inner race and rolling-element generate a periodic amplitude modulation at the period of the inner race and cage rotation respectively.

According to the above considerations, the vibration signal is generally taken as a signal in time domain in this work is taken as Discrete vibration signal $x(n)$, as shown in Fig. 1.

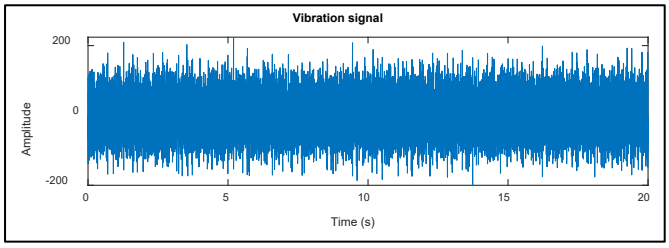

Fig. 1 Vibration signal in time domain considering in this work.

2.2. Cyclo-stationary signal processing

If the rotational speed remains constant while acquiring data, it is expected that rotating mechanical components will produce periodic transient patterns that exhibit cyclic behavior. The transmission of these signals frequently include data regarding the operational status of machine components. Signal processing and feature extraction techniques are commonly employed to extract this information and subsequently analyze the health condition of the machinery. According to the principles of cyclo-stationary theory, the signals obtained due to rotation of equipment are described by considering the first and second orders of cyclo-stationary. A signal is considered to possess cyclo-stationary of order n when its statistical n-order moment exhibits periodicity with a period of N. To illustrate, a signal demonstrates first-order cyclo-stationary (CS1) when its first moment (i.e. mean value) is a periodic function that follows Equation (1). Conversely, a stationary signal maintains a constant mean value at all times [36].

$$R_{1x}(n) = R_{1x}(n + N) = \mathbb{E}\{x(n)\} \quad (1)$$

Where:

$R_{1x}(n)$: First statistical moment.

$x(n)$: Discrete vibration signal.

$\mathbb{E}$: Ensemble averaging operator.

N : Period of periodic function.

n : The variable of time.

In the context of rotating machinery, the CS1 vibration signals can be described as periodic waveforms that are associated with components that are phase-locked with the rotor speed. These components may include issues such as shaft misalignment and spalling gears, etc. In contrast, a signal that exhibits cyclo-stationary of the second order (CS2) is characterized by periodicity in its second-order statistical moment [21]. Specifically, this pertains to statistical measures associated with energy intensity and flow. Instances of these signals encompass white noise signals that undergo amplitude modulation through a periodic signal. The instantaneous autocorrelation function effectively captures the 2nd-order statistics:

$$R_{2x}(n,\tau) = R_{2x}(n + N,\tau) = \mathbb{E}\{x(n)x(n-\tau)^*\} = \mathbb{E}\left\{x(n + \beta\tau)x\left(n - \overline{\beta}\tau\right)^*\right\} \quad (2)$$

Where: $\beta + \overline{\beta} = 1$

Typically, $\beta = \overline{\beta} = 0.5$ at symmetrically autocorrelation-function while $= 0$, $\overline{\beta} = 1$ for asymmetrically autocorrelation-function [37].

The vibration signals associated with bearings are commonly denoted as (CS2), as they exhibit an underlying periodicity that is closely linked to the rotational speed of the shaft. In signal analysis processes, n^{th}-order cyclo-stationary (CSn) refers to a signal that exhibits periodicity in its n^{th}-order statistical moment. However, the signals having orders greater than CS2 are typically disregarded, like CS1 and CS2 effectively capture the characteristics of interest in signals produced by rotating machinery. The sequential cyclic autocorrelation function has been observed to possess significant efficacy as a signal processing tool across various applications. In the case of signals derived from physical measures, like vibrations and acoustic signals, there are additional advantageous to utilize the corresponding frequency-domain-tool. The time-based autocorrelation-function $R_{2x}(n,\tau)$ is a mathematical function that depends on (n) and (τ). The frequency-domain counterpart of the given function is dependent on: (1) the cyclic frequency, denoted as (α) which is associated with the modifying signal, and (2) the spectral frequency, denoted as (f) which is associated with the carrier signal. The Cyclic Spectral Correlation (CSC) is a computational technique that effectively characterizes the CS1 and CS2 signals throughout the frequency-frequency domain [38]. The CSC can also be referred to the correlation distribution of the carrier and modulation frequencies of the signatures included in the signals, as described in equation (3), and Fig. 2 (b) shows the Cyclic Spectral Correlation (CSC).

$$S_{2X}(f,\alpha) = \lim_{W\to\infty}\frac{1}{W}\mathbb{E}\{\mathcal{F}_W[x(n)]\mathcal{F}_W[x(n+\tau)]^*\} = \mathbb{E}\left\{X(f + \beta\alpha)X\left(f - \overline{\beta}\alpha\right)^*\right\} \quad (3)$$

Where:

$S_{2X}(f,\alpha)$: the spectral correlation functions.

$\mathcal{F}_W[x(n)]$: Fourier transform of the signal $x(n)$ during a finite time interval W.

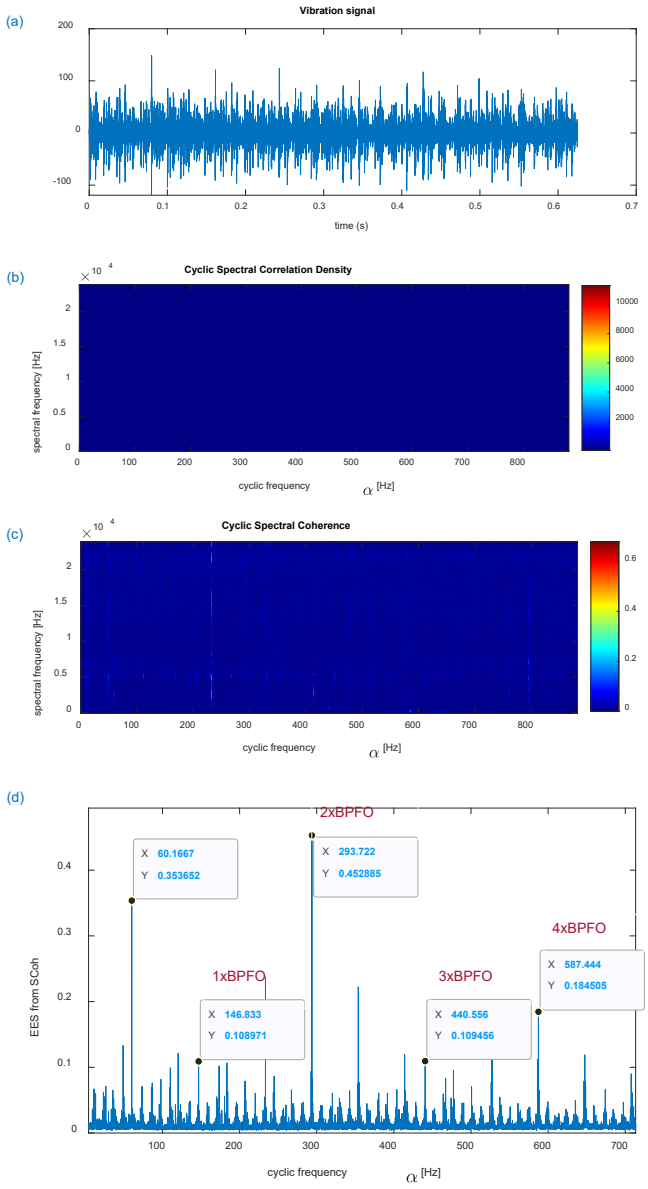

Fig. 2 The vibration analysis using spectral correlation in frequency-frequency domain.

2.3. Application of ACP for evaluating of spectral correlation

Assume signal with totally length (L) collected in interval of sampling $\Delta t = 1/Fs$. Given a symmetric processing window function of length *Nw*, Short-Time Fourier Transform (STFT) can be computed for a specific piece of signal in i^{th}-time. The values of Δt and length *Nw* are provided in equation (4). The complex envelope or complex demodulate is a collective term used to refer to the STFT coefficient [32].

$$X_{STFT}(i,f_k)=\sum_{m=0}^{N_w-1}x(iR+m)w(m)e^{-j2\pi mf_k\Delta t} \quad (4)$$

The symbol (f_k) denotes the discrete frequency, which is equal to $k\,\Delta f = k\,Fs/Nw$, where Δf is the frequency resolution, k is an integer, Fs is the sampling frequency, and Nw is the length of the tapering window denoted by $w(m)$. The variable R denotes the temporal displacement (measured in samples) between successive windows, or alternatively referred to as the decimation factor [32, 33]. The analysis of a signal is significantly influenced by the phase shift, making it crucial to adjust phase reference to initial point of signal [34].

$$Xw(i,f_k)=\sum_{m=0}^{Nw-1}x(iR+m)w(m)\,e^{-j2\pi(m+iR)f_k\Delta t} = \mathrm{X}_{STFT}(i,f_k)e^{-j2\pi iRf_k\Delta t} \quad (5)$$

The time smoothed cyclic periodogram, also known as the Averaged-Cyclic-Periodogram, is a highly effective estimator for spectral correlation. The Averaged-Cyclic-Periodogram is viewed extension of Welch's method, that use the averaging technique over brief overlapped periodograms in order to effectively compute the power-spectrum [39]. When the cyclic frequency α = 0, the output of the ACP aligns with Welch's estimator [37]. Equation (6) provides the expression for ACP in the context of asymmetric spectral correlation [34].

$$S_{2X}(f\,,\alpha)=\frac{1}{K\,||\,w\,||^2\,F_s}\sum_{i\,=\,0}^{k-1}X_w\,(i,f)\,X_w\,(i,f-\alpha)^* \quad (6)$$

The spectral-correlation is described by Eq. (7) by STFT-envelopes determining by FFT [34].

$$S_{2X}(f\,,\alpha)=\frac{1}{K\,||\,w\,||^2\,F_s}\sum_{i\,=\,0}^{k-1}X_{STFT}\,(i,f)\,X_{STFT}\,(i,f-\alpha)^*e^{-j2\pi iRf_k\Delta t} \quad (7)$$

Here, the variable K is defined as $\left(L-N_w+R\right)/R$, representing the count of blocks shifted by R with each block having a length of N_w. The term $||\,w\,||^2=\sum_{n=0}^{N_w-1}|\,w(n)|^2$ denotes the power of the window function. It is important to note that when N_w is a power of two or a similar approach is used for any N_w, the STFT coefficients are determined by the FFT. By shifting the time-domain-signal, first will allow you to calculate the frequency shifted coefficients [34].

$$X_{STFT}(i,f_k-\alpha)=\sum_{m\,=\,0}^{N_w-1}(x(iR+m)e^{j2\pi m\alpha\Delta t})\,w(m)e^{-j2\pi mf_k\Delta t} \quad (8)$$

It is important to acknowledge that if frequency shifting is implemented on complete time-domain-signal (where n = 0, 1, 2, 3, 4, ..., L) in order for preparing of the computation of the shifted spectrum, the resulted coefficients of Short-Time Fourier Transform (STFT) are adjusted for phase, rendering the term of exponential function in Equation (7) unnecessary.

The utilization of this word becomes necessary in the context of block wise application of frequency shifting. Therefore, the spectral correlation utilizing the phase corrected Short-Time-Fourier Transform is expressed by:

$$S_{2X}(f,\alpha)=\frac{1}{K\,||\,w\,||^2\,F_s}\sum_{i\,=\,0}^{k-1}X_{STFT}(i,f)X_{STFT}^{C}(i,f-\alpha)^* \quad (9)$$

The phase-compensated Short-Time-Fourier-Transform (STFT), denoted as $X_{STFT}^{C}(i,f-\alpha)$, is expressed by the subsequent equation:

$$X_{STFT}^{C}(i,f_k-\alpha)=\sum_{m\,=\,0}^{N_w-1}\left(x(iR+m)e^{j2\pi(iR+m)\alpha\Delta t}\right)w(m)e^{-j2\pi mf_k\Delta t} \quad (10)$$

According to the literature, the Averaged-Cyclic-Periodogram (ACP) has been identified as the utmost effective estimator [37]. The Averaged-Cyclic-Periodogram offers a high-resolution spectral correlation because to the ability to adjust the carrier frequency mesh Δf by utilizing a large N_w, while simultaneously keeping an acceptable cyclic frequency resolution $\Delta\alpha = Fs/L$. The ACP method entails the computation of the average of correlated STFT coefficients throughout the entire acquisition time T, which is equal to LTs. Here, to represents the interval of sampling. Conceptually, the averaging process is likened to low-pass filter having bandwidth of ($1/T$). Hence, the utilization of a decimation factor R enables the down sampling of complex envelopes while maintaining the integrity and dependability of the outcomes [33]. In order to optimize computing efficiency while minimizing cyclic leakage, multiple scholars have proposed setting the time shifting parameter R to a value more than 1 but less than N_w [37, 33, 40, 41]. When using the Hann or Hamming window, the value of R may be calculated as $N_w/3$, which corresponds to a 67% overlap. On the other hand, when using the half-sine window, the value of R can be determined as $N_w/2$, resulting in a 50% overlap. It is important to acknowledge that in cases when ($f - \alpha$) is below zero, the equations (6), (7), or (9) can be utilized to compute the correlation between positive (f) and negative ($f - \alpha$) frequencies. This case is commonly practice in the communication signal to uncover a characteristic related to twice carrier frequency, as outlined in references [42, 43]. Nevertheless, in the realm of mechanical-signal in vibration investigation, establishing correlation between negative frequencies is considered undesirable, as indicated by reference [34].

2.4. Evaluation of cyclic-spectral-coherence and improved envelope spectrum

The analysis of the cyclic-spectral-coherence generates in map of bi-variables allows for the identification of unseen modulations, rendering it reliable method to distinguish cyclo-stationary in vibration signals [34, 37]. To mitigate unequal distributions, it is possible to implement a whitening operation on the CSC. The Cyclic-Spectral-Coherence (CSCoh) is an expanded tool that characterizes the spectral correlations across a range of normalized values from 0 to 1. It is mathematically defined as Fig. 2(c) shows the Cyclic Spectral Coherence (CSCoh).

$$\mathrm{CSCoh}(\alpha, \mathrm{f}) = \frac{\mathrm{CSC_x}(\alpha, \mathrm{f})}{\sqrt{\mathrm{CSC_x}(0, \mathrm{f})\mathrm{CSC_x}(0, \mathrm{f}+\alpha)}} \quad (11)$$

The integration of both the CSC and CSCoh, bi-variable maps are performed with frequency-axis to yield a uniform spectrum. This integration process produces 1-D spectrum function, that is dependent on the cyclic frequency (α). The spectral frequencies to be integrated are characterized as including the entire accessible band, ranging (0-Nyquist) frequency. This integration yields spectrum which effectively captures totally modulations found in signal. Conversely, the band is characterized as the entity which optimizes the cyclic characteristic frequency of interest, whereas simultaneously reducing presence of background noise and other frequency components which could potentially obscure the desired frequency. By integrating over a specified band on the bi-variable map, the detecting rate of distinctive frequency associated with the existing signal damage can be enhanced. The spectrum that is obtained from the frequency-frequency domain, as described by Equation (12), is referred to as the Improved Envelope Spectrum (IES). Figure 2(d) shows the improved envelope spectrum.

$$\mathrm{IES}(\alpha) = \frac{1}{\mathrm{F_2} - \mathrm{F_1}} \int_{\mathrm{F_1}}^{\mathrm{F_2}} |\mathrm{CSCoh_x}(\alpha, \mathrm{f})| \mathrm{df} \quad (12)$$

2.5. Applying fast ACP to evaluate the spectral correlation

The ACP approach has several benefits, one of which is that the time shift (R) is independent of the desired range of cyclic frequency. Therefore, the memory required remains constant independent of the highest cyclic frequency that has to be scanned. In addition, it should be noted that the approach is a reliable estimator of spectral correlation with a constant time-frequency resolution product [32,37]. Yet, the substantial computational requirement restricts its practical use. Alsalaet has presented a fast ACP approach for efficiently calculating the accurate ACP [36]. In the following discussion, the focus will be on the asymmetric SC with β values of 0 and 1. To provide a thorough understanding of the fast algorithm, Fourier transform frequency shifting will be demonstrated to provide a complete view of the approach. The act of multiplying the time-domain signal by the rotating vector $exp(j2\pi f_0)$ is widely recognized as being similar to shifting in the frequency-domain by f_0, as written [44].

$$\mathcal{F}\{X(t)e^{j2\pi f_0 t}\} = \int_{-\infty}^{\infty} X(t)e^{j2\pi f_0 t}e^{-j2\pi f t}\, dt = \int_{-\infty}^{\infty} X(t)e^{-j2\pi(f-f_0)t}\, dt = X(f - f_0) \quad (13)$$

Figure 3 illustrates the impact of frequency shifting on the actual and imaginary components of the spectrum of a signal in real time. The spectrum of a real-valued signal in the negative frequency range is the complex conjugate of the spectrum in the positive frequency range. Shifting the frequency by f_0 makes the whole spectrum in the frequency domain to change, like line $(f - f_0)$ is relocated to line (f). In the context of Discrete Fourier Transform (DFT), applying the operation of pre-multiplying the signal by $exp(j2\pi\Delta f)$ causes a shift of the whole spectrum by one line. This means that the frequency component f_k -1 is relocated to f_k. The Fast-SC of Antoni et al. [34] has previously used this. Alsalaet [36] is attempting to use the frequency shifting property once again in order to compute ACP in an additional intelligent manner. Given that the overall signal length L is much larger than N_w, it follows that the cyclic frequency resolution Δα is considerably finer than the spectral frequency resolution Δf. Each spectral frequency spacing consists of N_b cyclic frequency lines, (N_b) is calculated as L divided by N_w and may be rounded to the closest integer for the Fast ACP application.

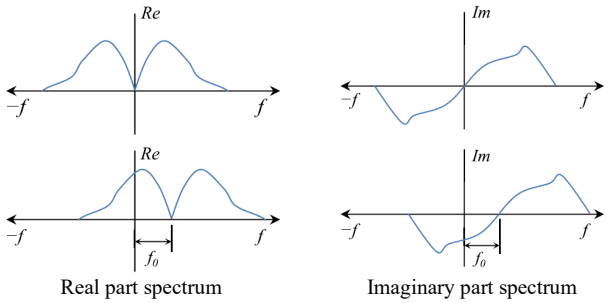

Fig. 3 Frequency shifting of spectrum of measured time-domain signal [34].

Figure 4 displays a portion of an amplitude spectrum. The bold lines indicate the spectral frequency lines, while the lighter lines denote their α-shifted counterparts. The value of α is determined by the equation α = p Δα, where p may take on values of 1, 2, 3, and so on, up to $N_b - 1$. The (N_b Δα) line corresponds to the spectral line that precedes it. The primary concept behind the fast ACP approach is the computation of the shifted spectra only for the N_b lines of α. To determine the shifted component of a certain frequency f_k beyond (N_b Δα), it may be derived from the previously shifted or unshifted lines. To illustrate, let's consider the task of calculating the component $X_{STFT}(i, f_k - \alpha)$, where $\alpha = (N_b + q)\,\Delta\alpha$. In this case, it can be obtained by shifting $f_k - 1$ by $q\Delta\alpha$ (since q is less than N_b), or by applying an appropriate phase correction to $X_{STFT}(i, f_k - 1 - q\Delta\alpha)$. Assume that the total number of cyclic frequency lines is $N_a = \alpha_{max}/\Delta\alpha$, then the computing advantage in calculating the shifted spectra is given by the ratio N_a/N_b. Further discussion will be provided on how to improve the technique and determine the total computational advantage.

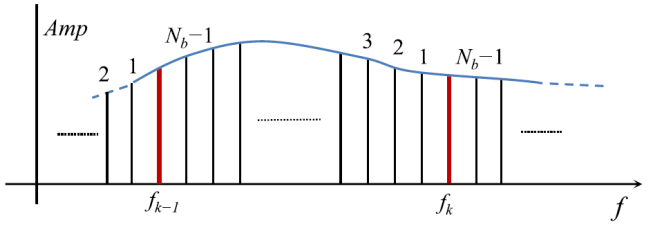

Fig. 4 Spectral lines and shifted counterparts [34].

2.6. Implementation of Fast-ACP

In this section, the procedure used to implement the Fast-ACP algorithm is described. The following steps are used.

Set and compute the following parameters: Input (L) totally length and (Fs) sampling frequency. For Hann window, choice N_w and set $R = N_w/3$. Given ($\Delta\alpha = Fs/L$), the total number of cyclic frequency lines ($N_a = \alpha_{max}/\Delta\alpha$), the number of cyclic frequency lines in one spectral spacing is ($N_b = L/N_w$). Compute the number of blocks ($K = (L - N_w + R)/R$).

Initial spectrogram calculation: Employ Eq. (9) to eradicate further phase correction, and then compute and store the unshifted spectrogram

$X_{STFT}(i, f_k)$, i = 0, 1, 2, …. (K–1) applying (FFT).

Compute of the shifted phase corrected spectra: For each block i, i = 0, 1, 2, …. (K–1), compute $X^C_{STFT}(i, f_k - \alpha)$, p = 1, 2, 3, 4…. ($N_b$ – 1), if $\alpha = p\Delta\alpha$ by FFT next to shift signal in time-domain.

For each block i, correlate $X_{STFT}(i, f_k)$ and $X^C_{STFT}(i, f_k - q\Delta\alpha)^*$, for the full spectral and cyclic frequency range if q = 1, 2, 3, 4…. (N_a). The shifted component at any cyclic frequency $q\Delta\alpha$ is estimated by:

$$S^c_{STFT}(i, f_k - q\Delta\alpha) = S^c_{STFT}(i, f_{k-m} - p\Delta\alpha)$$

If $m = \text{int}(q/N_b)$ and $p = \text{mod}(q/N_b)$.

If $k < m$, correlation is terminated for avoiding the negative frequencies in vibration signals. for each change in (m)'s or jumping between lines, a phase correction of function $exp(j2\pi iRN_b\Delta\alpha)$ must be used. For minimizing multiplications, the above correction linked with a variable $X_{STFT}(i, f_k)$ primarily and then gradually recalculated with each (m) transition.

After merging the correlated components when i = 0, 1, 2, 3, ……., (K–1), the results are corrected using Eq. (9) and $K\|w\|^2 Fs$ to calculate the spectral correlation. On other side, SCoh can be estimated using [37].

$$SCoh(f, \alpha) = \frac{S_{2x}(f, \alpha)}{\sqrt{S_{2x}(f, 0)S_{2x}(f - \alpha, 0)}}$$

Where $S_{2X}(f, 0)$ is estimated according to correlate $X_{STFT}(i, f_k)$ with its conjugate and $S_{2X}(f - \alpha, 0)$ is estimated according to correlate $X^C_{STFT}(i, f_k - \alpha)$ and its conjugate. Figure 5 illustrated the Fact ACP flow chart used in this work.

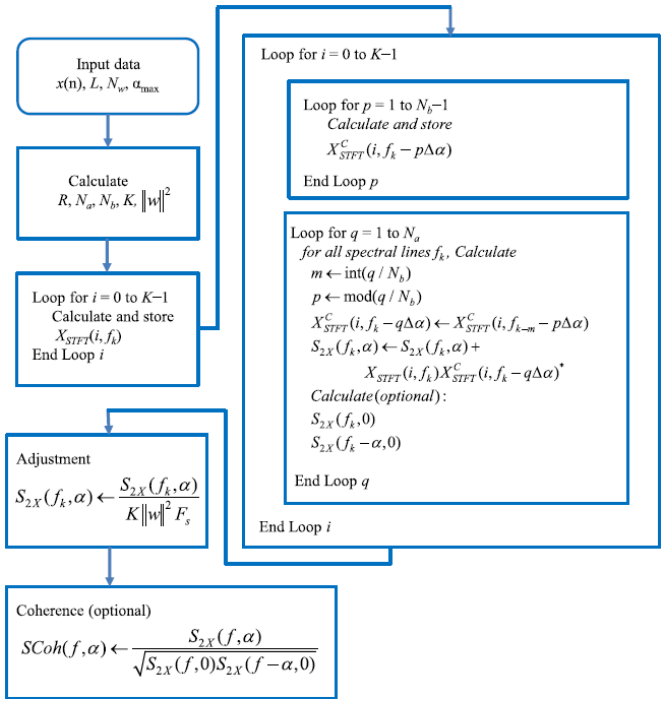

Fig. 5 Fast ACP method used in this work [36].

3. Experimental work

3.1. The machinery fault simulator (MFS)

The Machinery Fault Simulator (MFS) is a device utilized for the purpose of examining the main symptoms of frequent machinery breakdowns in a way that is both efficient and straightforward. Each component is precisely machined to strict specifications in order to ensure smooth operation without any detrimental vibration signal interference. In a controlled environment, the machinery fault simulator can be considered an effective tool for obtaining knowledge in machinery faults diagnostics, since it allows for the additional effects of many defects either separately or in combination. As depicted in Fig. 6, the spectra quest MFS found in the applied laboratory of the department of mechanical engineering at the university of Basrah was used and it consists of a 1 Hp variable frequency AC motor accompanied by a programmable controller including a multi-featured front panel. The controller allows for rpm adjustment within a range of 0 to 6000 rpm, allowing operation at various speeds. A tachometer equipped with an LCD display is employed for the purpose of measuring the rotational speed. A ¾ inch diameter steel shaft, equipped with a bearing loader weighing 11 pounds (5 kg) and two clamp collars for holding the bearing loader at the midpoint of the shaft. This arrangement is employed to apply loads and improve the spectrum amplitude of the system. Two split bracket bearing housings are designed to facilitate the process of changing experimental bearings. A flexible coupling is utilized to provide a connection between the motor and the shaft. An accelerometer of the B & K 4366 type, with a serial number of 0931214, was mounted to the experimental bearing housing.

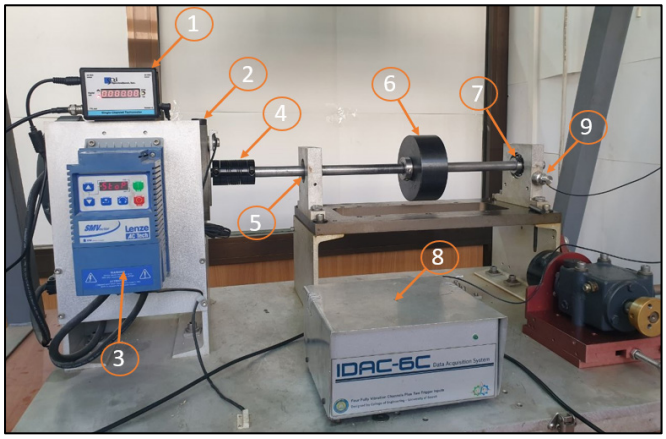

(1) Tachometer. (2) Electric motor.
(3) AC-motor controller. (4) Flexible coupling.
(5) Normal bearing. (6) Bearing loader.
(7) Experimental bearing. (8) Data acquisition.
(9) Accelerometer

Fig. 6 Machine fault simulator components.

3.2. Ball bearing used in this work

In this work, a 1205 double-row self-aligning ball bearing manufactured by Koyo is utilized. This type of bearing provides the advantage of compensating for misalignment and shaft deflection, making it appropriate for applications with significant levels of vibration or misalignment [45]. Moreover, it is easily assembled and disassembled, which simplifies the process of introducing defects into specific components of the bearing without damaging its integrity. Figure 7 illustrates the

bearing in its assembled state. The frequencies associated with bearing faults, termed bearing characteristic frequencies, depend on the bearing's dimensions and specifications. Table 1 shows the dimensions of the Koyo 1205 bearing along with the characteristic frequencies of its components (cage, inner race, outer race, balls).

Table 1. Koyo 1205C3 bearing specifications [45].

Parameter	Value
Inner diameter	25 mm
Outside diameter	52 mm
Ball diameter	7 mm
Bearing width	15 mm
Number of balls	24
Cage defect, FTF	0.41 × Shaft frequency
Ball defect, BSF	2.5687 × Shaft frequency
Outer race defect, BPFO	4.8907 × Shaft frequency
Inner race defect, BPFI	7.1092 × Shaft frequency

Fig. 7 Koyo bearing (1205C3) in its assembled condition.

3.3. Types of experimental faults

Artificial defects manufacturing is a widely used method of simulating defects in roller bearings for testing and analysis purposes, aiming to mirror real-world conditions. These fabricated defects can take different sizes and shapes. In this work, slots defects with 0.191 mm size are used. These defects are manufactured within each component of the ball bearing including the outer race, inner race, and balls as in Fig. 8.

Outer race slot Inner race slot

Ball slot

Fig. 8 Types of defects in the used ball bearing.

3.4. Experiment procedures

In this work, four types of ball-bearing defects, manufactured within the individual components of the ball-bearing such as the outer race, inner race, and balls as listed in Table 2 were used as the basis for collecting vibration data. This data was utilized for diagnosing defects using the spectral correlation technique under varying machine speed.

A data acquisition device was used to collect vibration signals of generated by the Machinery Fault Simulator (MFS). The following steps are used in experimental procedure, see Fig. 9.

1. Install a 5 kg disk was connected to the shaft to simulate load conditions, as illustrated in Fig. 6 of the test rig.
2. Additionally, install two bushings were installed on the ¾ inch shaft ends to fix the ball bearings by compensating for the diameter difference between the shaft and the internal diameter of the bearing.
3. Next, the operational settings for the data acquisition device (IDAC-6C) software interface were configured, as depicted in Fig. 10.
4. Vibration data is then gathered for both constant and varying speeds for both normal and faulty bearings. Finally, the collected raw vibration data were processed using MatLab software to assess the condition of the bearings.

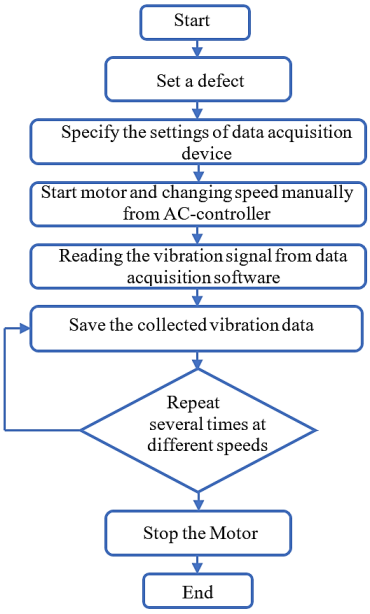

Fig. 9 Laboratory experimental procedures flow chart.

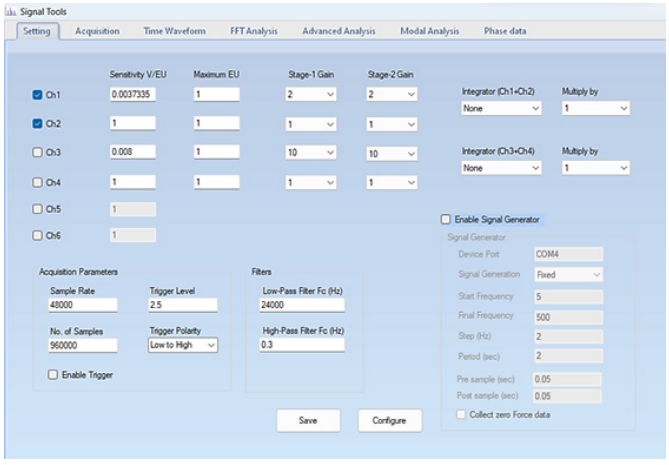

Fig. 10 Operation settings for IDAC-6C software interface.

Table 2. Total cases studied in this experimental work.

Defect Type	Defect Shape	Defect Size (mm)	Number of defects	Varying speed range in Acceleration Case (R.P.M)	Varying speed range in Deceleration Case (R.P.M.)
Normal	none	none	none	480-2040	---
Outer	slot	0.196	one slot	480-2040	---
Inner	slot	0.191	one slot	480-2040	---
Ball	slot	0.196	one slot	480-2040	---
Compound	slot	outer: 0.196 inner: 0.191 ball: 0.196	Three slots	480-2040	1800 - 660

4. Results and discussion

This paper presents the results and discussion of applying the spectral correlation technique, along with spectral coherence, and enhanced envelope spectra to analyze the real signals of ball bearings (specifically, Koyo 1205C3) under normal and defective (inner, outer, and ball) conditions. The data collected from the data acquisition device were processed using MatLab software (version R2022a) in both frequency-order domain and order-order domain for varying speed, two cases of varying speed are considered, the first one is acceleration case, the speed increases from (480-2040) rpm, i.e. (8-34 Hz), while the second case is deceleration case, the speed decreases from (1800-660) rpm, i.e. (30-11 Hz).

Firstly, the measured vibration and speed signals of acceleration and deceleration cases are illustrated in Figs. 11 and 12. The increasing or decreasing rate of speed appears sharply in both vibration and speed signals.

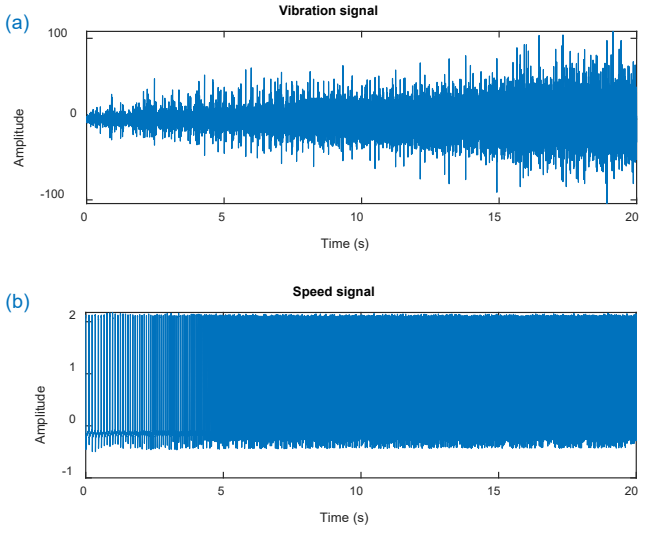

Fig. 11 Ball bearing signals in acceleration case (a) Vibration signal, and (b) Speed signal.

Secondly, the bi-variables maps of the ball bearing in conditions (normal, outer slot: size 0.196 mm, inner slot: size 0.191 mm, ball slot: size 0.196 mm) to estimate the characteristic frequencies and EES of acceleration case in frequency-order and order-order maps, and these frequencies and EES values are listed in Table 3 and 4.

In the third step, the compound defects condition (outer slot: size 0.196 mm, inner slot: size 0.191 mm, ball slot: size 0.196 mm) in acceleration and deceleration cases are measured and analyzed in this work.

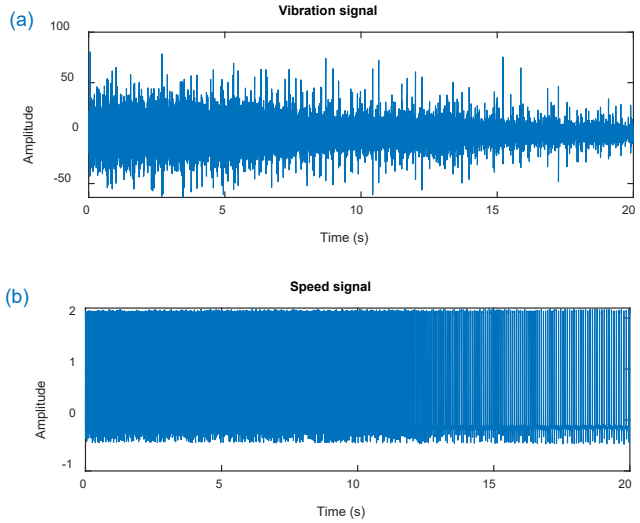

Fig. 12 Ball bearing signals in deceleration case (a) Vibration signal, and (b) Speed signal.

Table 3. The first three estimated values of characteristic frequencies and EES in frequency-order domain.

Bearing condition		Normal	Outer race defect	Inner race defect	Ball defect
Cyclic Frequency (order)	1	1.0000	4.8809	7.1189	2.5552
	2	2.0000	9.7642	14.2354	5.1082
	3	3.0000	14.6452	21.3570	7.6635
EES	1	0.0407	0.1249	0.2072	0.4430
	2	0.2455	0.4044	0.1507	0.3668
	3	0.0480	0.1038	0.1185	0.2472
Processing time (minute)		20.0733	22.0650	19.1183	21.0216

Table 4. The first three estimated values of characteristic frequencies and EES in order-order domain.

Bearing condition		Normal	Outer race defect	Inner race defect	Ball defect
Cyclic Frequency (order)	1	0.9991	4.8768	7.1105	2.5531
	2	1.9983	9.7536	14.2237	5.1039
	3	2.9974	14.6329	21.3368	7.6570
EES	1	0.0385	0.1790	0.2122	0.4286
	2	0.1918	0.3952	0.1237	0.4312
	3	0.0459	0.1048	0.0977	0.2556
Processing time (minute)		14.594	16.7700	12.9431	15.9259

Defects in a ball bearing are specific types of faults that occur within the particular component of the bearing. For the Koyo 1205 ball bearing, the Ball Pass Frequency Outer (BPFO) is expected to appear at 4.8907 times the rotating frequency, the Ball Pass Frequency Inner (BPFI) at 7.1092 times the rotating frequency, and the Ball Spin Frequency (BSF) at 2.5687 times the rotating frequency. These specific frequencies are essential for detecting potential defects on the outer race, inner race, and rolling elements (balls) respectively, thus facilitating early diagnosis of defects. The results of the acceleration case in frequency-order and order-order maps are illustrated in Figs. 13 and 14. In comparison, Figs. 15 and 16

show the frequency-order and order-order maps of the compound defects condition in the deceleration case. These figures depict the diagnostic results of a bearing operating under compound defect conditions, with each figure comprising multiple subfigures representing different stages of signal processing and analysis. The enhanced envelope spectrum reveals the characteristic cyclic frequencies of the outer race, inner race, and ball defects and thus the bearing condition can be diagnosed. Figures 13-16 and Tables 3 and 4 illustrate the appearance of peaks at the calculated (BPFO, BPFI, and BSF) values and their corresponding harmonics in the enhanced envelope spectrum under varying speeds. It is crucial to observe that within each spectrum, the presence of at least three harmonics indicates the presence of a fault, as shown by the experimental results. These findings demonstrate the effectiveness of the spectral correlation method in accurately detecting and diagnosing ball-bearing defects under varying machine speeds.

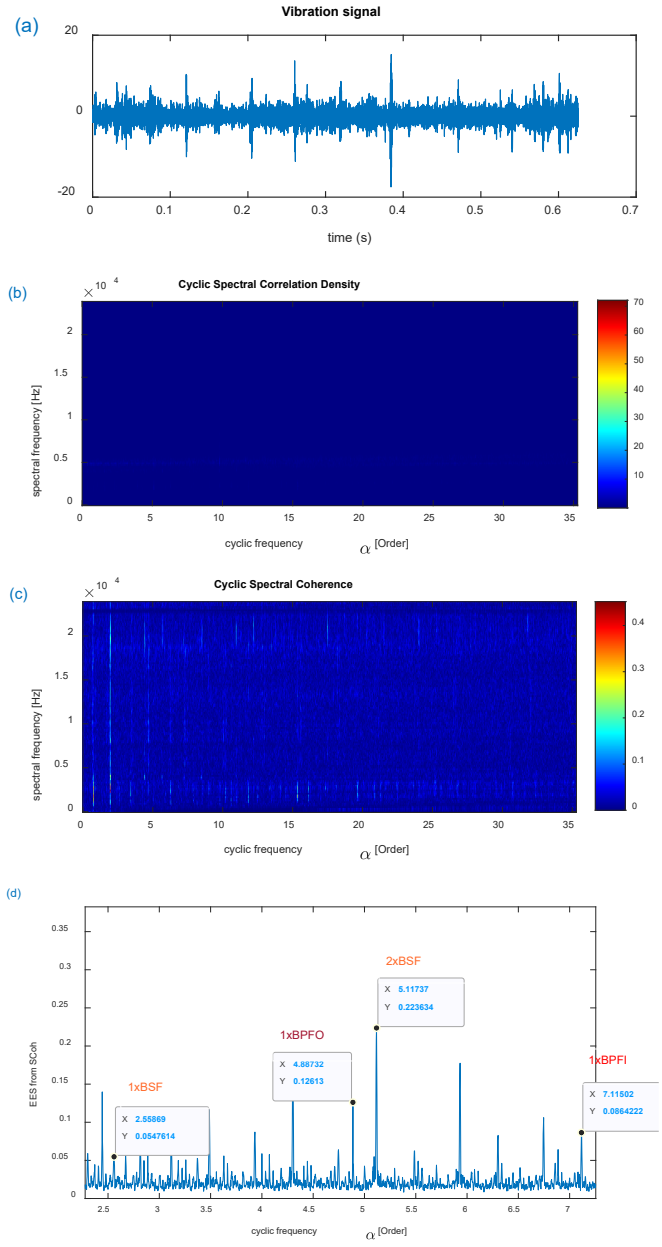

Fig. 13 Vibration analysis of compound defects of ball bearing in acceleration case using spectral correlation in frequency-order domain.

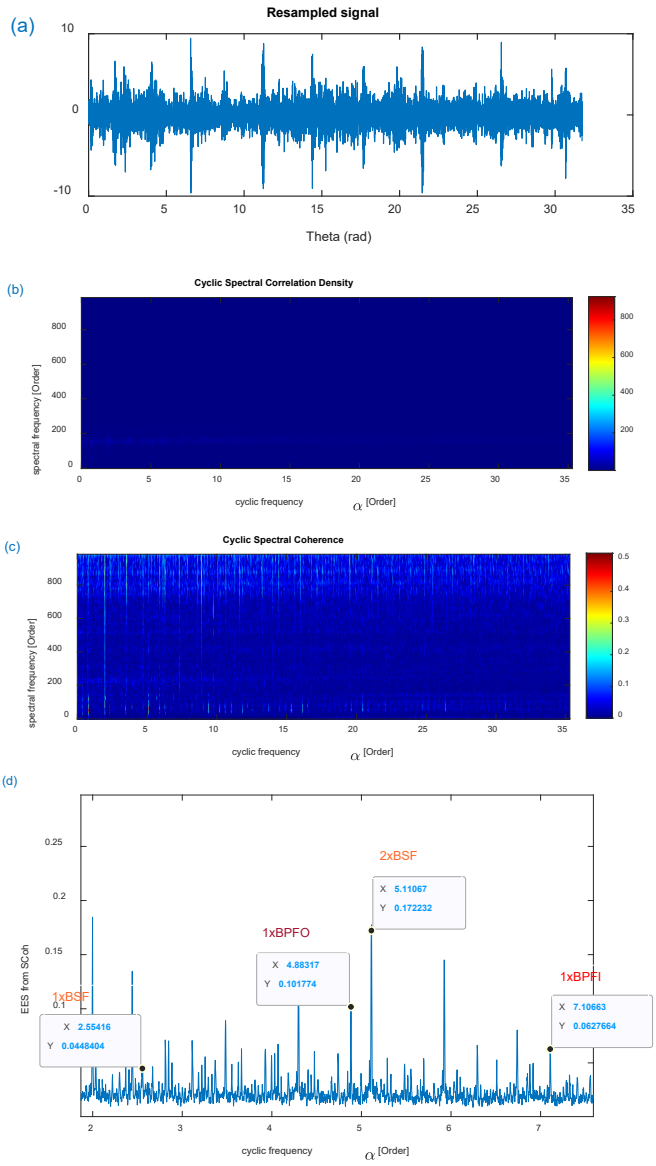

Fig. 14 Vibration analysis of compound defects of ball bearing in acceleration case using spectral correlation in order-order domain.

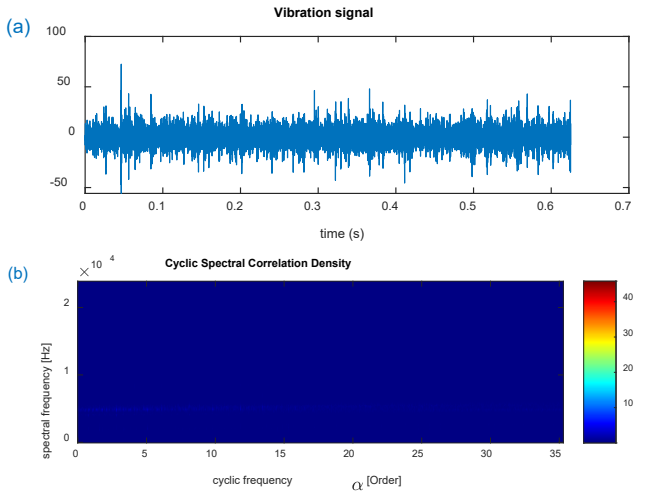

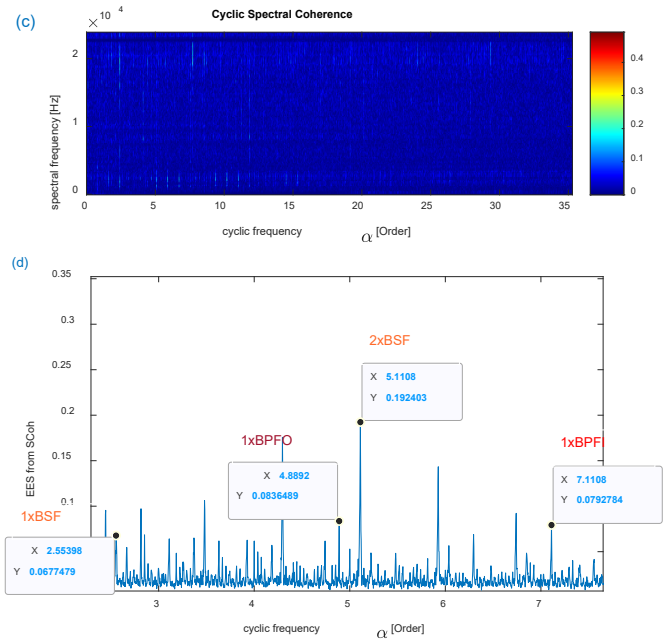

Fig. 15 Vibration analysis of compound defects of ball bearing in deceleration case using spectral correlation in frequency-order domain.

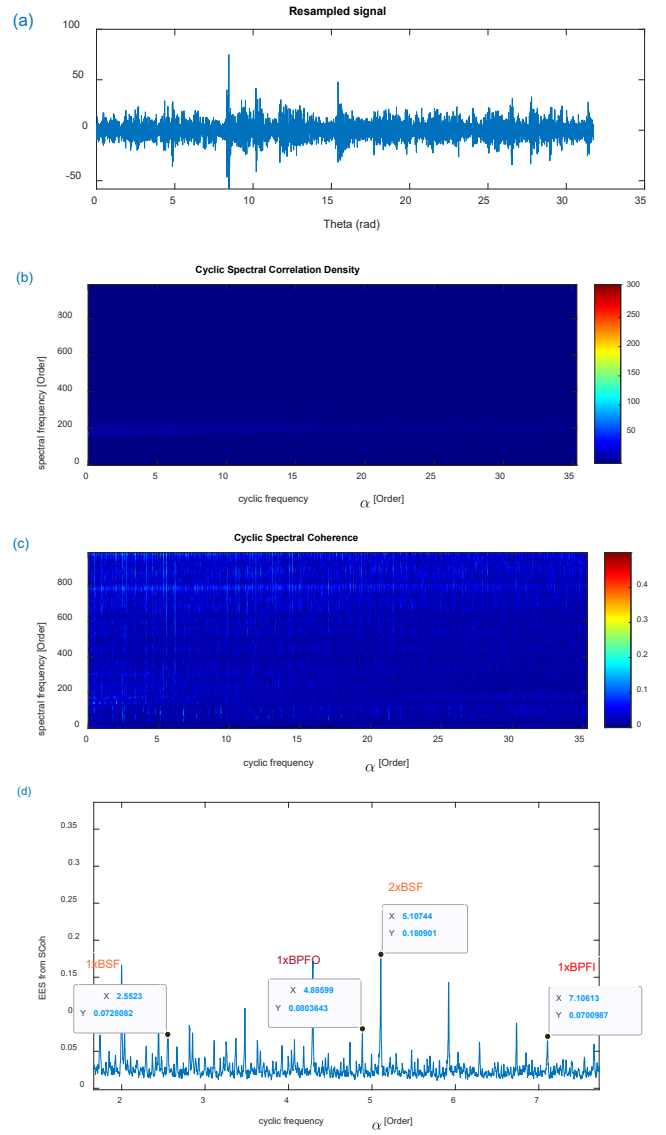

Fig. 16 Vibration analysis of compound defects of ball bearing in deceleration case using spectral correlation in order-order domain.

5. Conclusions

In this work, Fast-ACP method was used to increase speed of analyzing and diagnosing the defects in ball bearing (Koyo 1205C3 type) under varying speed condition. Four types of defects were studied, the slot in outer race with size 0.196 mm, the slot in inner race with size 0.191 mm, in ball with size 0.196 mm in additional to compound defect. The machinery fault simulator (MFS) equipment was used to determine ball bearing defects using vibration signal analysis. Also, spectral correlation technique was employed to detect defects in ball bearings running at varying speed, along with spectral coherence and the corresponding Enhanced Envelope Spectrum (EES) in frequency-order domain and order-order domain. The following points can be concluded:

1. The characteristic frequencies estimated by bi-variables maps of the ball bearing (Koyo 1205C3 type) under conditions (normal, outer slot: size 0.196 mm, inner slot: size 0.191 mm, ball slot: size 0.196 mm) are very close to that calculated in Koyo web (BPFO: 4.8907, BPFI: 7.1092, BSF: 2.5687).
2. The applied method computation advantage increases as the cyclic frequency range increases and does not require large memory, making it suitable for low-memory platforms such as portable data collectors.
3. The variable speed tests have shown that the OOSC provides comparable, if not better, results when compared to FOSC. This supports the inference that OOSC can successfully replace FOSC in analyzing cyclo-non-stationary signals and hence gives a benefit to Fast-ACP.

Abbreviations	Abbreviations
ACP	Averaged Cyclic Periodogram
FastACP	Fast Averaged Cyclic Periodogram
FFT	Fast Fourier Transform
EES	Enhanced Envelope Spectrum
MFS	Machinery Fault Simulator
CS	Cyclo-stationary
CS1	First-Order Cyclo-stationary
CS2	Second Order Cyclo-stationary
FOSC	Frequency-Order Spectral Correlation
OOSC	Order-Order Spectral Correlation
FAM	FFT Accumulation Method
SSCA	Strip-Spectral-Correlation Algorithm
FSC	Fast-Spectral-Correlation
STFT	Short Time Fourier Transform
CSC	Cyclic Spectral Correlation
CSCoh	Cyclic-Spectral-Coherence
DFT	Discrete Fourier Transform
BPFO	Ball Pass Frequency Outer race
BPFI	Ball Pass Frequency Inner race
BSF	Ball Spin Frequency

References

[1] Y. Li, K. Ding, G. He, X. Jiao, "Non-stationary vibration feature extraction method based on sparse decomposition and order tracking for gearbox fault diagnosis," Measurement, Vol. 124, pp. 453-469, 2018. https://doi.org/10.1016/j.measurement.2018.04.063

[2] Y. Zhu, S. Tang, L. Quan, W. Jiang, L. Zhou, "Extraction method for signal effective component based on extreme-point symmetric mode decomposition and Kullback-Leibler divergence," Journal of the Brazilian Society of Mechanical Sciences and Engineering, Vol. 41, No. 100, 2019. https://link.springer.com/article/10.1007/s40430-019-1599-9

[3] Y. Lei, J. Lin, M. J. Zuo, Z. He, "Condition monitoring and fault diagnosis of planetary gearboxes: A review," Measurement, Vol. 48, pp. 292-305, 2014. https://doi.org/10.1016/j.measurement.2013.11.012

[4] Y. Zhu, P. Qian, S. Tang, W. Jiang, W. Li, J. Zhao, "Amplitude-frequency characteristics analysis for vertical vibration of hydraulic AGC system under nonlinear action," AIP Advances, Vol. 9, Issue 3, 2019. https://doi.org/10.1063/1.5085854

[5] Y. Zhu, S. Tang, C. Wang, W. Jiang, X. Yuan, Y. Lei, "Bifurcation characteristic research on the load vertical vibration of a hydraulic automatic gauge control system," Processes, Vol. 7, Issue 10, 2019. https://doi.org/10.3390/pr7100718

[6] J. Antoni, D. Abboud, G. Xin, Cyclostationarity in Condition Monitoring: 10 Years After; ISMA 2016 Including; ISMA USD: Leuven, Belgium, pp. 2365-2376, 2016.

[7] D. Abboud, S. Baudin, J. Antoni, D. Remond, M. Eltabach, O. Sauvage, "The Spectral Analysis of Cyclo-Non-Stationary Signals," Mechanical Systems and Signal Processing, Vol. 75, pp. 280-300, 2016. https://doi.org/10.1016/j.ymssp.2015.09.034

[8] X. Zhang, Z. Bao, "The analysis and processing of non-stationary signal," China Natl. Def. Ind. Press, pp. 325-351, 1998.

[9] S. Tang, S. Yuan, Y. Zhu, "Data Preprocessing Techniques in Convolutional Neural Network based on Fault Diagnosis towards Rotating Machinery," IEEE Access, Vol. 8, pp. 149487-149496, 2020. https://doi.org/10.1109/ACCESS.2020.3012182

[10] P. Borghesani, J. Antoni, "A faster algorithm for the calculation of the fast spectral correlation," Mechanical Systems and Signal Processing, Vol. 111, pp. 113-118, 2018. https://doi.org/10.1016/j.ymssp.2018.03.059

[11] C. Capdessus, M. Sidahmed, J. L. Lacoume, "Cyclostationary Processes: Application in Gear Faults Early Diagnosis," Mechanical Systems and Signal Processing, Vol. 14, Issue 3, pp. 371-385, 2000. http://dx.doi.org/10.1006/mssp.1999.1260

[12] I. Antoniadis, G. Glossiotis, "Cyclostationary analysis of rolling-element bearing vibration signals," Journal of Sound and Vibration, Vol. 248, Issue 5, pp. 829-845, 2001. https://doi.org/10.1006/jsvi.2001.3815

[13] R. B. Randall, J. Antoni, S. Chobsaard, "The relationship between spectral correlation and envelope analysis in the diagnostics of bearing faults and other cyclostationary machine signals," Mechanical Systems and Signal Processing, Vol. 15, Issue 5, pp. 945-962, 2001. https://doi.org/10.1006/mssp.2001.1415

[14] J. Antoni "Cyclic spectral analysis of rolling-element bearing signals: Facts and fictions," Journal of Sound and Vibration, Vol. 304, Issue 3-5, pp. 497-529, 2007. https://doi.org/10.1016/j.jsv.2007.02.029

[15] Z. K. Zhu, Z. H. Feng, F. R. Kong, "Cyclostationarity analysis for gearbox condition monitoring: Approaches and effectiveness," Mechanical Systems and Signal Processing, Vol. 19, Issue 3, pp. 467-482, 2005. https://doi.org/10.1016/j.ymssp.2004.02.007

[16] A. C. McCormick, A. K. Nandi, "Cyclostationarity in rotating machine vibrations," Mechanical Systems and Signal Processing, Vol. 12, Issue 2, pp. 225-242, 1998. https://doi.org/10.1006/mssp.1997.0148

[17] G. Dalpiaz, A. Rivola, R. Rubini, "Effectiveness and sensitivity of vibration processing techniques for local fault detection in gears," Mechanical Systems and Signal Processing, Vol. 14, Issue 3, pp. 387-412, 2000. https://doi.org/10.1006/mssp.1999.1294

[18] J. Antoni, J. Daniere, F. Guillet, "Effective vibration analysis of ic engines using cyclostationarity. Part I-A methodology for condition monitoring," Journal of Sound and Vibration, Vol. 257, Issue 5, pp. 815-837, 2002. https://doi.org/10.1006/jsvi.2002.5062

[19] J. Antoni, R. B. Randall, "Differential diagnosis of gear and bearing faults," Journal of Vibration and Acoustics, Vol. 124, Issue 2, pp. 165-171, 2002. https://doi.org/10.1115/1.1456906

[20] J. Antoni, R. B. Randall, "A stochastic model for simulation and diagnostics of rolling element bearings with localized faults," Journal of Vibration and Acoustics, Vol. 125, Issue 3, pp. 282-289, 2003. https://doi.org/10.1115/1.1569940

[21] J. Antoni, F. Bonnardot, A. Raad, M. El Badaoui, "Cyclostationary modeling of rotating machine vibration signals," Mechanical Systems and Signal Processing, Vol. 18, Issue 6, pp. 1285-1314, 2004. https://doi.org/10.1016/S0888-3270(03)00088-8

[22] R. Zimroz, W. Bartelmus, "Gearbox condition estimation using cyclo-stationary properties of vibration signal," Key Engineering Materials, Vol. 413-414, pp. 471-478, 2009. https://www.scientific.net/KEM.413-414.471

[23] J. Antoni, "Cyclostationarity by examples," Mechanical Systems and Signal Processing, Vol. 23, Issue 4, pp. 987-1036, 2009. https://doi.org/10.1016/j.ymssp.2008.10.010

[24] W. A. Gardner, A. Napolitano, L. Paura, "Cyclostationarity: Half a century of research," Signal Process, Vol. 86, Issue 4, pp. 639-697, 2006. https://doi.org/10.1016/j.sigpro.2005.06.016

[25] J. Urbanek, T. Barszcz, R. Zimroz, J. Antoni, "Application of averaged instantaneous power spectrum for diagnostics of machinery operating under non-stationary operational conditions," Measurement, Vol. 45, Issue 4, pp. 1782-1791, 2012. https://doi.org/10.1016/j.measurement.2012.04.006

[26] J. Urbanek, T. Barszcz, J. Antoni, "Time-frequency approach to extraction of selected second-order cyclostationary vibration components for varying operational conditions," Measurement, Vol. 46, Issue 4, pp. 1454-1463, 2013. https://doi.org/10.1016/j.measurement.2012.11.042

[27] D. Abboud, J. Antoni, M. Eltabach, S. Sieg-Zieba, "Angle \ time cyclostationarity for the analysis of rolling element bearing vibrations," Measurement, Vol. 75, pp. 29-39, 2015. https://doi.org/10.1016/j.measurement.2015.07.017

[28] A. Mauricio, W. A. Smith, R. B. Randall, J. Antoni, K. Gryllias, "Improved Envelope Spectrum via Feature Optimisation-gram (IESFOgram): A novel tool for rolling element bearing diagnostics under non-stationary

operating conditions," Mechanical Systems and Signal Processing, Vol. 144, 2020. https://doi.org/10.1016/j.ymssp.2020.106891
[29] J. Li, Q. Yu, X. Wang, Y. Zhang, "An enhanced rolling bearing fault detection method combining sparse code shrinkage denoising with fast spectral correlation," ISA Transactions, Vol. 102, pp. 335-346, 2020. https://doi.org/10.1016/j.isatra.2020.02.031
[30] B. Zhang, Y. Miao, J. Lin, H. Li, "Weighted envelope spectrum based on the spectral coherence for bearing diagnosis," ISA Transactions, Vol. 123, pp. 398-412, 2022. https://doi.org/10.1016/j.isatra.2021.05.012
[31] W. A. Smith, P. Borghesani, Q. Ni, K. Wang, Z. Peng, "Optimal demodulation band selection for envelope-based diagnostics: A comparative study of traditional and novel tools," Mechanical Systems and Signal Processing, Vol. 134, 2019. https://doi.org/10.1016/j.ymssp.2019.106303
[32] R. S. Roberts, W. A. Brown, H. H. Loomis, "Computationally efficient algorithms for cyclic spectral analysis," IEEE Signal Processing Magazine, Vol. 8, Issue 2, pp. 38-49, 1991. https://doi.org/10.1109/79.81008
[33] W. A. Brown, H. H. Loomis, "Digital implementations of spectral correlation analyzers," IEEE Transactions on Signal Processing, Vol. 41, Issue 2, pp. 703-720, 1993. https://doi.org/10.1109/78.193211
[34] J. Antoni, G. Xin, N. Hamzaoui, "Fast computation of the spectral correlation," Mechanical Systems and Signal Processing, Vol. 92, pp. 248-277, 2017. https://doi.org/10.1016/j.ymssp.2017.01.011
[35] P. Borghesani, J. Antoni, "A faster algorithm for the calculation of the fast spectral correlation," Mechanical Systems and Signal Processing, Vol. 111, pp. 113-118, 2018. https://doi.org/10.1016/j.ymssp.2018.03.059
[36] J. K. Alsalaet, "Fast Averaged Cyclic Periodogram method to compute spectral correlation and coherence," ISA Transactions, Vol. 129, Part B, pp. 609-630, 2022. https://doi.org/10.1016/j.isatra.2022.01.029
[37] J. Antoni, "Cyclic spectral analysis in practice," Mechanical Systems and Signal Processing, Vol. 21, Issue 2, pp. 597-630, 2007. https://doi.org/10.1016/j.ymssp.2006.08.007
[38] A. Mauricio, W. A. Smith, R. B. Randall, J. Antoni and K. Gryllias, "Improved Envelope Spectrum via Feature Optimisation-gram (IESFOgram): A novel tool for rolling element bearing diagnostics under non-stationary operating conditions," Mechanical Systems and Signal Processing, Vol. 144, 2020. https://doi.org/10.1016/j.ymssp.2020.106891
[39] P. Welch, "The use of fast Fourier transform for the estimation of power spectra: A method based on time averaging over short, modified periodograms," IEEE Transactions on Audio and Electroacoustics, Vol. 15, Issue 2, pp. 70-73, 1967. https://doi.org/10.1109/TAU.1967.1161901
[40] R. Boustany, J. Antoni, "Cyclic spectral analysis from the averaged cyclic periodogram," IFAC Proceedings Volumes, Vol. 38, Issue 1, pp. 166-171, 2005. https://doi.org/10.3182/20050703-6-CZ-1902.00028
[41] W. Gardner, "Measurement of spectral correlation," IEEE Transactions on Acoustics, Speech, and Signal Processing, Vol. 34, Issue 5, pp. 1111-1123, 1986. https://doi.org/10.1109/TASSP.1986.1164951
[42] J. F. Adlard, "Frequency Shift Filtering for Cyclostationary Signals," Ph.D. thesis, University of York, 2000.
[43] T. V. R. O. Camara, A. D. L. Lima, B. M. M. Lima, A. I. R. Fontes, A. D. M. Martins, L. F. Q. Silveira," Automatic modulation classification architectures based on cyclostationary features in impulsive environments," IEEE Access, Vol. 7, pp. 138512-138527, 2019. https://doi.org/10.1109/ACCESS.2019.2943300
[44] W. A. Gardner, "Exploitation of spectral redundancy in cyclostationary signals," IEEE Signal Processing Magazine, Vol. 8, Issue 2, pp. 14-36, 1991. https://doi.org/10.1109/79.81007
[45] https://koyo.jtekt.co.jp/en/products/detail/?pno=1205